

Simulation on mechanochemical coupling of rotary biomotors F_1 and V_1

Liqiang Dai(戴立强), Yao-Gen Shu(舒咬根), and Zhong-Can Ouyang(欧阳钟灿)
Citation: Chin. Phys. B, 2026, 35 (**2**): 028702. DOI: 10.1088/1674-1056/ae2674
http://cpb.iphy.ac.cn; http://iopscience.iop.org/cpb

What follows is a list of articles you may be interested in

RLsite: Integrating 3D-CNN and BiLSTM for RNA-ligand binding site prediction

Yan Zou(邹艳), Lang Yang(杨浪), Yanhui Liu(刘艳辉), and Yuyu Feng(冯玉宇)
Chin. Phys. B, 2025, 34 (**8**): 088709. DOI: 10.1088/1674-1056/adea9b

Dynamics of zebrafish locomotion being independent of spatial size

Zhen Wang(王震), Jian Gao(高见), Yongshang Long(龙永尚), Huaping Lv(吕华平), and Qun Wang(王群)
Chin. Phys. B, 2025, 34 (**3**): 038702. DOI: 10.1088/1674-1056/ada54c

Cross-correlations between signal's components

Quankun Zhao(赵全坤), Sen Li(李森), Changgui Gu(顾长贵), Haiying Wang(王海英), and Huijie Yang(杨会杰)
Chin. Phys. B, 2025, 34 (**2**): 028702. DOI: 10.1088/1674-1056/ad9ffb

Improving performance of screening MM/PBSA in protein-ligand interactions via machine learning

Yuan-Qiang Chen(陈远强), Yao Xu(徐耀), Yu-Qiang Ma(马余强), and Hong-Ming Ding(丁泓铭)
Chin. Phys. B, 2025, 34 (**1**): 018701. DOI: 10.1088/1674-1056/ad8ecb

Effects of individual heterogeneity on social contagions

Fu-Zhong Nian(年福忠) and Yu Yang(杨宇)
Chin. Phys. B, 2024, 33 (**5**): 058705. DOI: 10.1088/1674-1056/ad225e

---

Simulation on mechanochemical coupling of rotary biomotors F_1 and V_1

Liqiang Dai(戴立强)[1], Yao-Gen Shu(舒咬根)[1,†], and Zhong-Can Ouyang(欧阳钟灿)[2,‡]

[1] *Wenzhou Institute, University of Chinese Academy of Sciences, Wenzhou* 325000, *China*
[2] *Institute of Theoretical Physics, Chinese Academy of Sciences, Beijing* 100190, *China*

(Received 1 October 2025; revised manuscript received 17 November 2025; accepted manuscript online 2 December 2025)

The F_1-ATPase and V_1-ATPase are rotary biomotors. Alignment of their amino acid sequences, which originate from bovine heart mitochondria (1BMF) and *Enterococcus hirae* (3VR6), respectively, demonstrates that the segment forming the ATP catalytic pocket is highly conserved. Single-molecule experiments, however, have revealed subtle differences in efficiency between the F_1 and V_1 motors. Here, we perform both atomistic and coarse-grained molecular dynamics simulations to investigate the mechanochemical coupling and coordination in F_1 and V_1 ATPase. Our results show that the correlation between conformational changes in F_1 is stronger than that in V_1, indicating that the mechanochemical coupling in F_1 is tighter than in V_1. Moreover, the unidirectional rotation of F_1 is more processive than that of V_1, which accounts for the higher efficiency observed in F_1 and explains the occasional backward steps detected in single-molecule experiments on V_1.

Keywords: rotary biomotor, correlation, mechanochemical coupling, simulation

PACS: 87.16.Nn, 87.15.ap, 87.15.hp

DOI: 10.1088/1674-1056/ae2674 **CSTR:** 32038.14.CPB.ae2674

1. Introduction

Molecular motors are protein enzymes that directly convert chemical energy into mechanical work and can be divided into linear motors and rotary motors. Rotary motors, such as F_1-ATPase and V_1-ATPase, are usually reversible, that is, they can also synthesize ATP by utilizing the torque generated by their transmembrane companions. On the other hand, the mechanochemical coupling of rotary motors is tight, so that their efficiency is close to 100%. This efficiency is significantly higher than that of artificial motors, which is the main reason why many physicists study the mechanism of mechanochemical coupling in biomotors.[1–11]

F_1F_o-ATPase is a ubiquitous enzyme that uses the transmembrane electrochemical potential to synthesize ATP in bacteria, chloroplasts, and mitochondria. The holoenzyme is a complex composed of two rotary motors, F_o and F_1 (see Fig. 1(a)). F_o consists of a "stator" (subunit a) and a "rotor" (the channel-forming "c-ring"), while F_1 comprises an $\alpha_3\beta_3$ stator and a central γ rotor (see Fig. 1(b)). The two stators are fixed by subunits $b_2\delta$, and the two rotors are coupled by subunit ε. The membrane-embedded F_o unit efficiently converts the proton motive force (p.m.f.) into mechanical rotation of the rotor, thereby inducing cyclic conformational changes in the $\alpha_3\beta_3$ crown of F_1 and driving ATP synthesis (see Fig. 1(c)). A striking characteristic of this motor is its reversibility: it may rotate in the reverse direction to hydrolyze ATP and utilize the released energy to pump protons across the membrane.[3,12–15]

V_1V_o-ATPase is structurally similar to F_1F_o-ATPase, as shown in Fig. 1(a). It is also a two-domain complex consisting of the soluble peripheral V_1 domain, responsible for ATP hydrolysis, and the membrane-embedded V_o domain, responsible for proton translocation. V_1 consists of catalytic subunits forming an A_3B_3 crown and a rotor axle (subunit D, see Fig. 1(b)), while V_o comprises the proton channel subunit a and a ring of proteolipid subunits (c-ring). The two stators are fixed by two peripheral stalk subunits (EG), and the two rotors are coupled by subunits dF.[16]

F_1F_o-ATPase and V_1V_o-ATPase showcase the evolutionary adaptation of rotary motors to perform specific cellular functions. While F_1F_o-ATPase is optimized for ATP synthesis in mitochondria, V_1V_o-ATPase is specialized for proton pumping in intracellular vesicles, organelles, and the extracellular milieu. F_1F_o-ATPase generates ATP by utilizing the transmembrane proton gradient in mitochondria, whereas V_1V_o-ATPase consumes ATP to maintain pH homeostasis at both the cellular and organismal levels.[3,17]

The key motif of mechanochemical coupling in rotary motors such as F_1/V_1-ATPase is the β/A subunit. It converts the energy released from ATP hydrolysis into rotor rotation through ergodic sampling of its conformational states. Single-molecule experiments have revealed subtle differences between the F_1 and V_1 motors, such as the torque generated

†Corresponding author. E-mail: shuyaogen@ucas.ac.cn
‡Corresponding author. E-mail: oy@itp.ac.cn

© 2026 Chinese Physical Society and IOP Publishing Ltd. All rights, including for text and data mining, AI training, and similar technologies, are reserved.

during rotation. The torque generated by F_1 reaches about 40 pN·nm, which is comparable to the free energy released from ATP hydrolysis under physiological conditions. As a result, the efficiency is estimated to be close to 100%, and the motor rotates processively at a speed of about 130 r.p.s.[18] In contrast, the torque produced by V_1 is about 30–35 pN·nm, backward steps occur occasionally, and the rotation speed is about 107 r.p.s.[19–22]

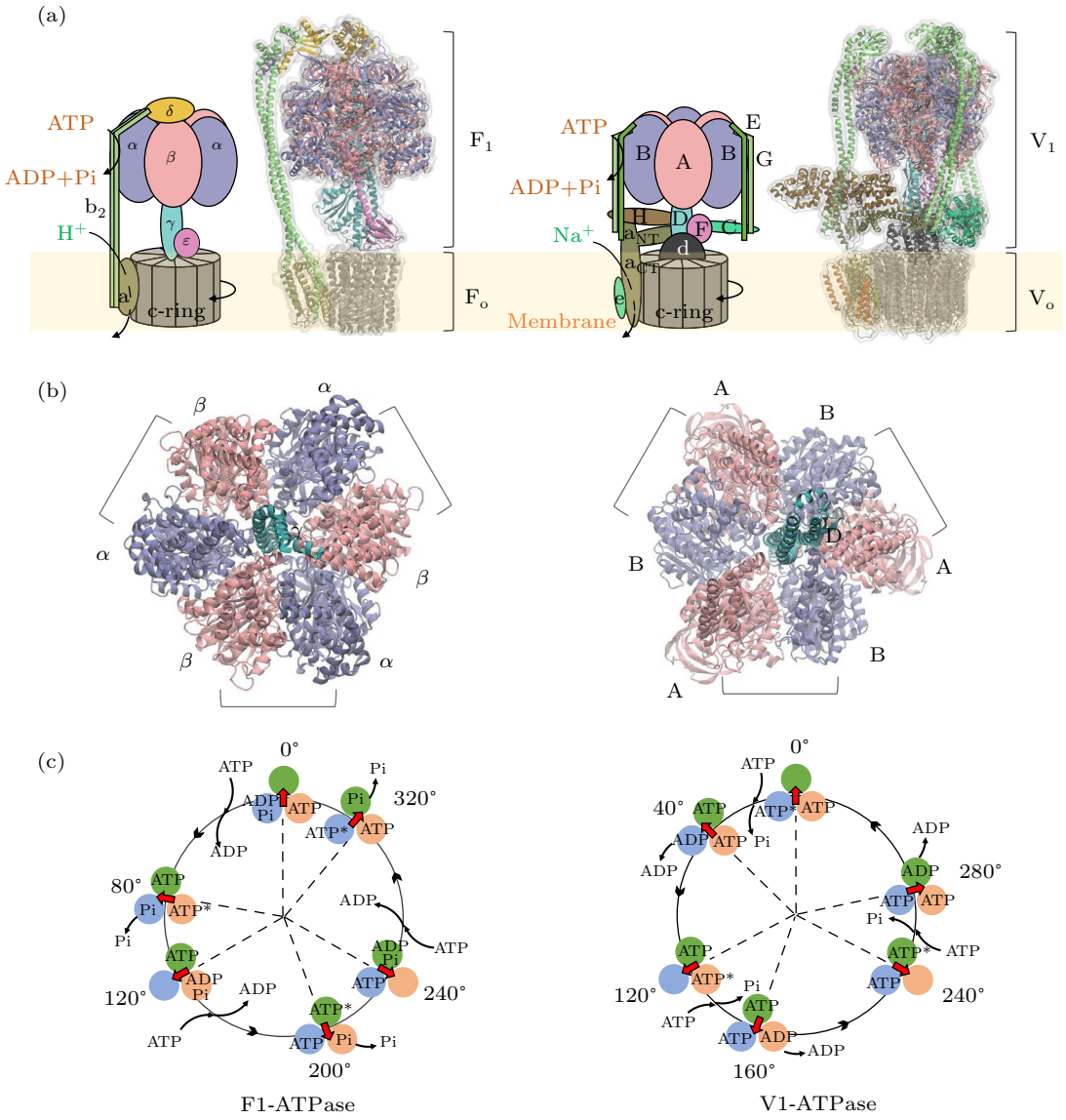


Fig. 1. Structures and ATP-hydrolysis substeps of rotary motors.[23–26] (a) Schematic illustrations and structures of F_1F_o-ATPase and V_1V_o-ATPase. The right motor is composed of a soluble catalytic core V_1 motor (A_3B_3D) and a membrane-embedded V_o motor (a–d–c-ring). Their stators are fixed by two peripheral stalks (EG), while the rotors are coupled by subunit F. The left motor is structurally similar to the right one. The F_1 ($\alpha_3\beta_3\gamma$) and F_o motors (a–c-ring) are connected by one peripheral stalk ($b_2\delta$) for the two stators and by the ε subunit for the two rotors, respectively. (b) Structures of the F_1 motor ($\alpha_3\beta_3\gamma$) and the V_1 motor (A_3B_3D). (c) Intermediate states in the ATP hydrolysis cycle and their corresponding rotational substeps of the motors.

The subtle differences in torque output between F_1-ATPase and V_1-ATPase may reflect their distinct biological functions and mechanistic features within the ATPase family. Understanding these differences can provide valuable insights into cellular energy conversion and the regulation of biochemical processes. Comparative studies of the mechanochemical coupling in these motors may also contribute to the development of novel therapeutics targeting ATPase activity in various diseases. Here, we conduct both atomistic molecular dynamics and coarse-grained simulations to investigate the coordination mechanisms in F_1 and V_1 ATPase.

2. Methods

2.1. Setup of atomistic MD simulations

All-atom MD simulations were performed using the NAMD 2.10 software[27] with the AMBER99SB_ILDN force field.[28] The initial structures of F_1-ATPase and V_1-ATPase were obtained directly from the crystal structures deposited in the Protein Data Bank under accession codes 1BMF[14] and

3VR6,[29] respectively.

Before MD simulations, the protein–nucleotide complex was solvated with TIP3P water in a cubic box, and the minimum distance from the complex to the box wall was set to 7 Å. The systems were neutralized with Na^+ and Cl^- ions to an ionic concentration of 0.15 M. All simulations were conducted under periodic boundary conditions. The van der Waals (vdW) and short-range electrostatic interactions were truncated at a cutoff distance of 12 Å. The particle-mesh Ewald (PME) method was employed to treat long-range electrostatic interactions.[30] The solvated systems were first energy-minimized using the steepest-descent algorithm, followed by a 10 ps MD simulation under the microcanonical (NVE) ensemble with a time step of 1 fs. Subsequently, a 5 ns equilibration under the canonical (NVT) ensemble and another 5 ns equilibration under the isothermal–isobaric (NPT) ensemble were performed with a time step of 1 fs, during which position restraints were applied to the heavy atoms of the proteins. In the constant-temperature simulations, the temperature was maintained at 300 K using the velocity-rescaling method.[31] The pressure was set to 1 bar using the Parrinello–Rahman barostat.[32] Finally, unconstrained 150 ns equilibrium simulations or targeted MD simulations were carried out under the NPT ensemble with a time step of 2 fs.[33]

2.2. Targeted MD simulations

The key motif of mechanochemical coupling in rotary motors F_1/V_1-ATPase is the conformational change of the β/A subunit induced by ATP binding. To accelerate the open–closed conformational transition of F_1/V_1, targeted molecular dynamics (TMD) simulations were employed.[34–36] In the targeted MD simulations, the open conformation of the α–β/A–B subunits was guided toward a final "target" closed structure by means of steering forces, mimicking the effect of ATP binding. At each time step, the root-mean-square (RMS) distance between the current coordinates and the target structure was computed after aligning the target structure to the current coordinates. The force acting on each atom is given by the gradient of the potential

$$U_{\mathrm{TMD}} = \frac{1}{2}\frac{k}{N}(\mathrm{RMS}(t) - \mathrm{RMS}^*(t))^2, \tag{1}$$

where $\mathrm{RMS}(t)$ is the instantaneous best-fit RMS distance between the current and target coordinates, and $\mathrm{RMS}^*(t)$ evolves linearly from the initial RMSD at the first TMD step to the final RMSD at the last TMD step. The spring constant k is scaled by the number N of targeted atoms.

2.3. Coarse-grained simulations

The coarse-grained (CG) simulations were performed using the CafeMol 3.0 software.[37] The initial structures of the F_1- and V_1-ATPase complexes were obtained from the Protein Data Bank with accession codes 1BMF and 3VR6, respectively. The Go model was employed for protein coarse graining,[38] in which each coarse-grained particle corresponds to the C_α atom of a single amino acid residue. Interactions between different subunits incorporated excluded-volume effects as well as electrostatic forces. All simulations were performed using Langevin dynamics.

To facilitate conformational transitions in the F_1- and V_1-ATPase complexes, a multiple-basin potential approach[39] was employed in the CG simulations (see Fig. 2). The multiple-basin energy potential is defined based on the eigenvalues derived from the characteristic equation

$$\begin{pmatrix} V_{\mathrm{G_o}+}(\boldsymbol{R}|\boldsymbol{R}_1) & \Delta \\ \Delta & V_{\mathrm{G_o}+}(\boldsymbol{R}|\boldsymbol{R}_2)+\Delta V \end{pmatrix} \begin{pmatrix} c_1 \\ c_2 \end{pmatrix} = V_{\mathrm{MB}} \begin{pmatrix} c_1 \\ c_2 \end{pmatrix}. \tag{2}$$

In this formulation, (i) $V_{\mathrm{G_o}+}(\boldsymbol{R}|\boldsymbol{R}_\gamma)$ corresponds to the off-lattice Go potential proposed by Clementi *et al.*[38] (ii) The parameter Δ serves as a coupling constant that smooths the transition between the two Go models; increasing Δ reduces the height of the energy barrier separating the two conformational basins. (iii) The parameter ΔV modulates the relative energy levels of the two basins, thereby influencing their stability.

Detailed descriptions of the simulation setup and workflow are provided in our previous work.[40]

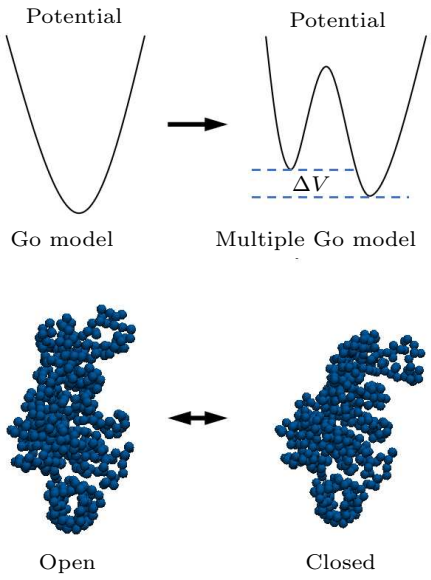


Fig. 2. Multiple-basin Go model potential. Comparison of the potentials (top) between the single-basin Go model and the multiple-basin Go model, and comparison of the two local minimum-energy structures (bottom) of the F_1 β subunit.

3. Results

3.1. Mechanochemical coupling in F_1 and V_1 ATPase

The $\alpha_3\beta_3$/A_3B_3 crown is tightly coupled to the rotor γ/D in the F_1/V_1 motor. Upon ATP binding, conformational

changes in the catalytic sites drive the rotation of the central shaft. To investigate the mechanochemical coupling mechanism, TMD simulations were performed for both F_1 and V_1 ATPases. During the simulations, the central shaft rotates by a certain angle when the conformation of one of the three active sites transitions from the open state to the closed state. The initial crystal structures of F_1 and V_1 correspond to the open–closed–closed configuration. Artificial steering forces were applied to the initially open site, enforcing its conformational transition to the closed state. The conformational changes of the initially open site toward the reference closed conformation are shown in Fig. 3(a) and 3(b).

To confirm the conformational changes on a longer timescale, we conducted CG simulations. The CG protein was constructed using the Go model, in which each amino acid is represented by a single bead. Both electrostatic interactions and volume-based repulsive interactions are taken into account, although explicitly incorporating detailed hydrogen bonding in CG simulations remains challenging.

The rotation of the central shaft also occurred on the longer timescale (μs) in the coarse-grained simulations, as shown in Fig. 3(c). A multiple–Go model was applied to the initially open site of the F_1 and V_1 ATPase. The conformation of the open site transitioned to the closed conformation when the potential was switched to the stable closed-state potential. Subsequently, the central shaft rotated by a certain angle after the open site became closed.

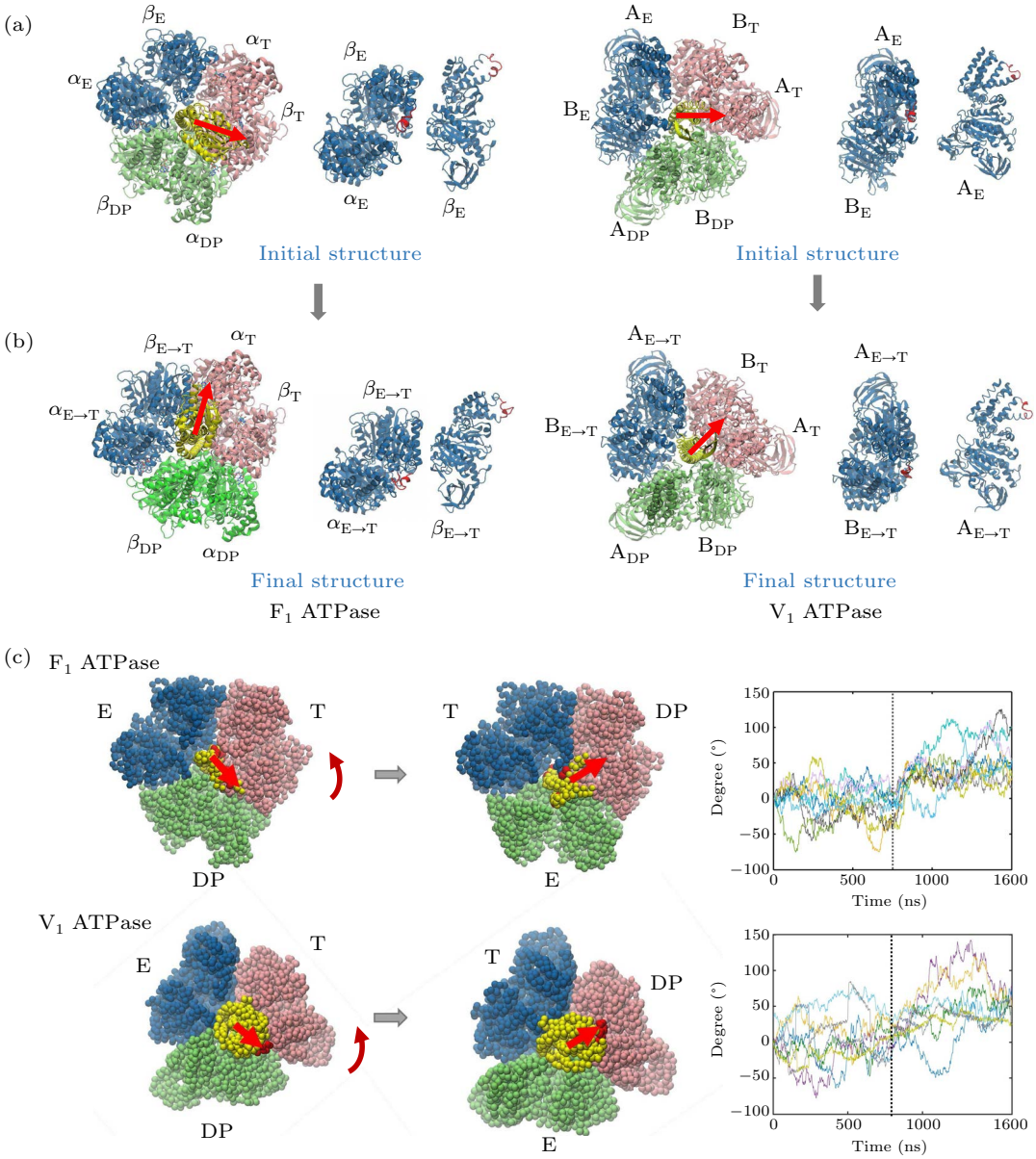


Fig. 3. Simulations of mechanochemical coupling in F_1 and V_1 ATPase using atomistic (a), (b) MD and coarse-grained (c) simulations. Top views of F_1 (left) and V_1 (right) ATPase are shown at the beginning and at the end of the MD simulations. The initially open site (colored blue) was enforced to undergo a conformational transition to the closed state during the simulations. The direction of the central shaft is indicated by an arrow. The rotational substep occurs at the dashed line, which marks the time point of the conformational transition. The subscripts E, T, and DP represent the empty (open), ATP-bound (closed), and ADP-bound (closed) states, respectively.

3.2. The coordination in crown of F_1 and V_1 subunits

According to the "binding change mechanism",[12] ATP binding to the open site triggers a series of cascading conformational changes, which manifest as rotor rotation with discrete substeps, as shown in Fig. 3. To study the mechanochemical coupling within the stator, we calculated the correlation coefficients between each subunit and the enforced catalytic site of the crown, and investigated how mechanical responses propagate from the ATP-binding E (empty) site to the corresponding DP (ADP-bound, closed) site and T (ATP-bound, closed) site in the stator of F_1. Specifically, we calculated residue-level correlations with the E-site ATP-binding residues (αI343, αR373, βG161–V164, βY345, βA421, βF424, and βT425), which are primarily located on the β_E subunit. This was achieved by first evaluating the pairwise cross-correlation values for all residues and then summing the correlation strengths between each subunit and the E-site ATP-binding residues. Near the E site, the resulting correlations were similarly high for both $\alpha_{E\to T}$ and $\beta_{E\to T}$ subunits, respectively (see Fig. 4).

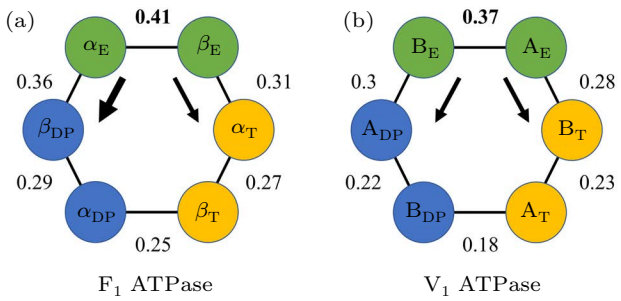


Fig. 4. Coordination transduction in the crowns of F_1 (left) and V_1 (right) ATPases. A steering force was imposed on the open catalytic site ($\alpha_E\beta_E$ for F_1 or A_EB_E for V_1). The calculated correlation coefficients between each pair of neighboring subunits are indicated.

We further calculated subunit-wise correlations to quantitatively describe the relationship between the enforced catalytic site (E→T site) and each subunit. To this end, we first computed the pairwise correlations for all residues. The correlation coefficient between each pair of residues was determined using the Pearson correlation coefficient[41]

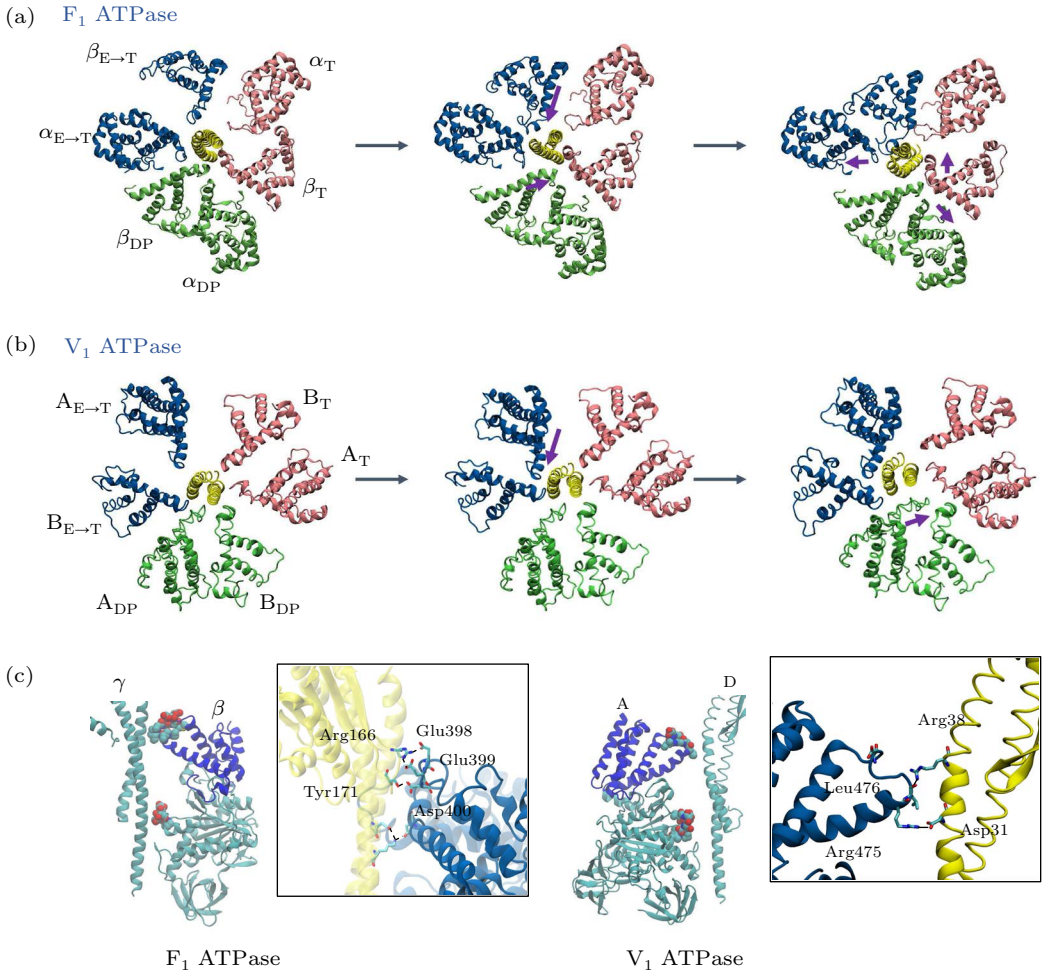


Fig. 5. Molecular details of central shaft rotation in F_1 (top) and V_1 (middle) ATPases. Closure of β_E enforces the counter-clockwise movement of the other two β subunits. The interactions between β and γ subunits are illustrated (top). Closure of A_E induces the counter-clockwise movement of only A_{DP}. The C-terminal interactions between A and D subunits are illustrated (middle). Bottom: Comparison of coupling in F_1 (left) and V_1 (right). Hydrogen bonding between β_E/A_E subunits and γ/D subunits is shown.

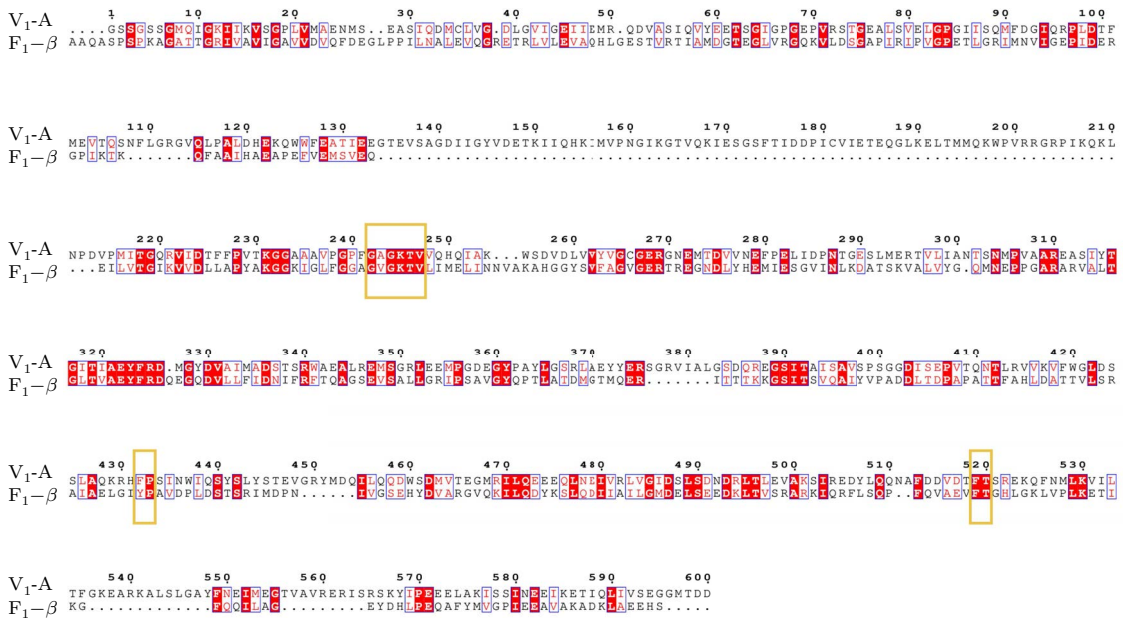


Fig. 6. Sequence alignment of the A subunit (V_1) and the β subunit (F_1). Conserved residues are highlighted in red, and residues in the ATP catalytic pocket that directly contact nucleotides are indicated with yellow boxes; these residues are highly conserved. The sequences of V_1 and F_1 are derived from crystal structures with PDB IDs 3VR6 and 1BMF, respectively.

$$C_{ij} = \frac{\langle (\boldsymbol{R}_i - \langle \boldsymbol{R}_i \rangle) \cdot (\boldsymbol{R}_j - \langle \boldsymbol{R}_j \rangle) \rangle}{\sqrt{\langle (\boldsymbol{R}_i - \langle \boldsymbol{R}_i \rangle)^2 \rangle \cdot \langle (\boldsymbol{R}_j - \langle \boldsymbol{R}_j \rangle)^2 \rangle}}, \tag{3}$$

where $\boldsymbol{R}_i$ is the position vector of the C_α atom of residue i, and $\langle \cdots \rangle$ denotes the average over the simulation trajectory. This procedure yields a pairwise $N \times N$ correlation matrix, where N is the total number of residues.

Finally, we calculated the correlation coefficient between subunit A and subunit B by[42]

$$C_{\mathrm{AB}} = \frac{\sqrt{\sum_{i \in \mathrm{subunitA}} \sum_{j \in \mathrm{subunitB}} C_{ij}^2}}{200}, \tag{4}$$

here, 200 is the empirical normalization factor.

The same calculation was carried out in V_1. The results are shown in Fig. 4. In both F_1 and V_1 motors, the two subunits of the enforced open site showed a higher correlation. Notably, in F_1 ATPase, a significant correlation was observed that facilitates unidirectional rotation. A higher correlation counterclockwise pathway from E→DP was found in F_1 ATPase, whereas a subtle difference in correlation in V_1 ATPase between E→DP and E→T appears.

The correlation remained high as it propagated from $\alpha_{\mathrm{E}\to\mathrm{T}}$ to β_{DP}, owing to an a-loop region (αQ405–D411) on the top of $\alpha_{\mathrm{E}\to\mathrm{T}}$ that interacts closely with the DELSEED region (βD394–D400) from β_{DP} and a helix underneath (βD383–M390) (see Fig. 5). Indeed, upon ATP binding to the E-site, the counterclockwise movement of the β_{DP} helix and DELSEED region pulled the γ shaft to rotate, thereby causing the β_{DP} protrusion movement. On the other hand, the propagation from $\beta_{\mathrm{E}\to\mathrm{T}}$ to α_{T} and then to β_{T} occurred over a comparatively long distance, and the correlation decayed noticeably toward β_{T}. Since the ADP/ATP binding site is mainly located on the β-subunit, it is reasonable that the upstream T-site is affected less than the downstream DP-site by E-site ATP binding.

The rotation of the central shaft is due to the push and pull of the C-terminal domain of the active subunit. The closing of the active site makes the C-terminal domain enclose the central shaft. In F_1-ATPase, the closing of the β_{E} subunit induced a pull force on the central shaft γ via the DELSEED region in the C-terminal domain. This pull force rotated γ by a certain degree in the counterclockwise direction. The C-terminal β_{DP} was also dragged by the rotation of γ (see Fig. 5). After the counterclockwise movement of $\beta_{\mathrm{E}\to\mathrm{T}}$ and β_{DP}, $\alpha_{\mathrm{E}\to\mathrm{T}}$ and α_{DP} moved outward slightly, and β_{T} moved counterclockwise. Nearly all the subunits in the crown were influenced by the closing of the β_{E} subunit, indicating tight coupling and unidirectionality. In contrast, in V_1, the conformational change of $A_{\mathrm{E}} \to A_{\mathrm{T}}$ only induced A_{DP} counterclockwise movement (see Fig. 5), indicating weaker coupling.

3.3. ATP catalytic pocket is highly conserved

The sequences of the V_1 A subunit and the F_1 β subunit were compared using sequence alignment with CLUSTALW,[43] and visualized using ESPript.[44] They exhibit 68% sequence similarity (see Fig. 6). The amino acids that directly contact the nucleotide (ATP catalytic pocket) are almost identical in F_1 and V_1. The high sequence similarity indicates that the evolution of F_1 and V_1 is highly conserved, and that they undergo similar conformational changes and share the same chemical hydrolysis mechanism.

4. Discussion

We conducted both atomistic and coarse-grained molecular dynamics simulations to investigate the mechanochemical coupling and coordination in F_1 and V_1 ATPase. Our results show that the correlation between conformational changes in F_1 is stronger than that in V_1, indicating that the mechanochemical coupling in F_1 is tighter than in V_1, which explains why the efficiency of F_1 is higher. Moreover, the unidirectional conformational changes in the F_1 crown were revealed based on the calculated correlation coefficients, indicating that the rotation of F_1 is more processive than that of V_1, which accounts for the occasional backward steps observed in single-molecule experiments of V_1. These differences likely result from evolutionary adaptations for diverse functions across species.

The substep of the central shaft was measured during CG simulations for F_1 and V_1 ATPase. After the initial transition of the E-site from the open to the closed conformation, the shaft rotated counterclockwise. Coarse-grained simulations can capture the rotational motion of the central shaft over longer time scales, addressing the short time-scale limitations of all-atom simulations. They also validate the rotational torque generated by conformational changes in the crown subunits acting on the central shaft. It should be pointed out that the substep resulting from CG simulation is only about 40° (see Fig. 3), which is much smaller than the 120° measured in single-molecule experiments. We summarize the following three main limitations of the simulation that contribute to the gap between theory and experiment:

(i) We simulated the overall conformational changes of the $\alpha\beta$ subunits following ATP binding. The primary conformational change observed was the closing motion of the C-terminus. However, subtle changes at the ATP binding site and their effects were not adequately captured;

(ii) Amino acids are simplified to single particles, accounting only for van der Waals repulsion and basic electrostatic interactions between subunits, while critical hydrogen bond interactions are neglected. Consequently, the breaking and reformation of hydrogen bonds between subunits are difficult to capture in coarse-grained simulations;

(iii) The simplification of particles and their interactions, such as electrostatic and van der Waals forces, weakens the forces between subunits, making it difficult for conformational changes to propagate to surrounding subunits as they would in a real biological system.

With the improvement of computing power, we aim to overcome these limitations and narrow the gap with more detailed simulations.

Appendix A: Calculation procedures of inter-subunit correlation

Firstly, the Pearson correlation coefficient between each pair of residues was computed using Eq. (3) based on molecular dynamics (MD) trajectories. For instance, considering the F_1-ATPase $\alpha_3\beta_3$ ring, which comprises 2860 residues, a 2860×2860 pairwise correlation matrix was generated according to Eq. (3), as shown in Fig. A1.

However, the Pearson correlation coefficient alone is insufficient to quantitatively capture the correlation between two subunits. Therefore, we introduced an artificial metric by calculating the RMS of all pairwise correlations between residues belonging to the two subunits under consideration. For example, to evaluate the inter-subunit correlation between α_{DP} and α_T, the RMS of all Pearson correlation coefficients within the designated triangular region of the correlation matrix (as illustrated in the figure) was computed in accordance with Eq. (4).

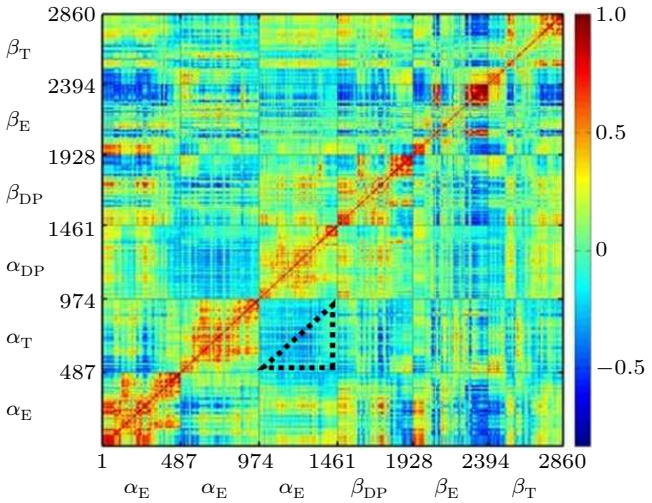


Fig. A1. The Pearson correlation matrix of the F1 crown is depicted in the diagram. The *x*- and *y*-axes correspond to the residue indices, while the color gradient indicates the magnitude of the correlation coefficients.

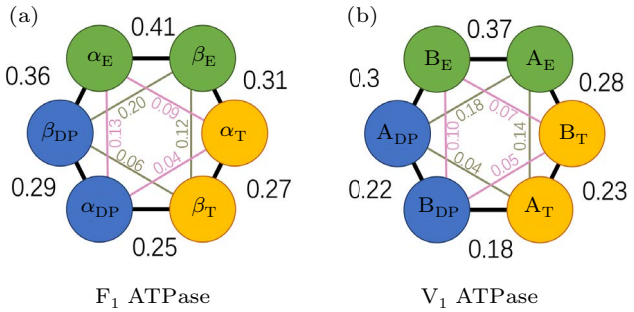


Fig. A2. Inter-subunit correlation from atomistic MD simulations. Correlations among individual α and β subunits within F_1-ATPase, as well as between A and B subunits in V_1-ATPase, were analyzed. The β and A subunits exhibit greater responsiveness to significant conformational changes and nucleotide binding in F_1 and V_1. Notably, correlation values for the β subunits surpass those of the α subunits in F_1-ATPase; similarly, in V_1-ATPase, correlations among A subunits are higher than those among B subunits.

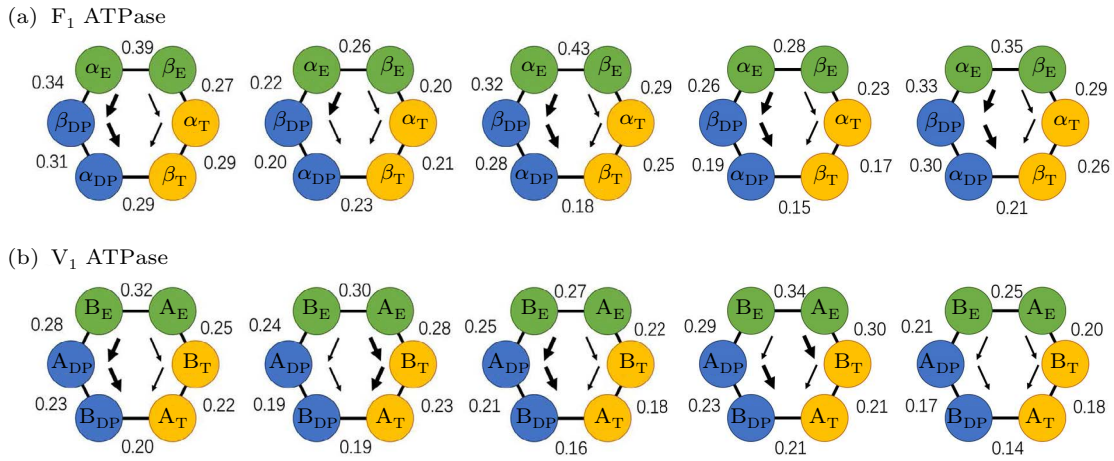


Fig. A3. Inter-subunit correlation within F_1 (upper) and V_1 (lower) ATPase from CG simulations. The correlation maps further corroborate the findings from molecular dynamics (MD) simulations. Specifically, a pronounced counterclockwise correlation pathway from the E to DP subunit is observed in F_1 ATPase, whereas the directional pattern in V_1 ATPase is less distinct.

Acknowledgments

This work was supported by the National Natural Science Foundation of China (Grant Nos. 22193032 and 32401033) and the Research Fund of Wenzhou Institute, Chinese Academy of Sciences (Grant Nos. WIUCASQD2020009, WIUCASQD2023005, XSZD2024004, 2021HZSY0061, and WIUCASICTP2022).

References

[1] Li M and Shu Y G 2020 *Physics of Soft and Condens Matter, The strategy of development of Chinese disciplines, Part. III, The Chap. 5: Biomotors* (Beijing: China Science Publishing & Media Ltd.) (in Chinese)
[2] Shu Y G and Ou-Yang Z C 2022 *Biophys. Rev. Lett.* **17** 43
[3] Shu Y G and Lai P Y 2008 *J. Phys. Chem. B* **112** 13453
[4] Shu Y G, Yue J C and Ou-Yang Z C 2010 *Nanoscale* **2** 1284
[5] Shu Y G, Zhang X H, Ou-Yang Z C and Li M 2012 *J. Phys.: Condens. Matter* **24** 035105
[6] Li M, Ou-Yang Z C and Shu Y G 2016 *Acta Phys. Sin.* **65** 188702 (in Chinese)
[7] Li M, Ou-Yang Z C and Shu Y G 2018 *Int. J. Mod. Phys. B* **32** 1840001
[8] Shu Y G and Shi H L 2004 *Phys. Rev. E* **69** 021912
[9] Ma R 2013 *Phys. Rev. E* **87** 052718
[10] Wang Z Q, Li J F, Xie Y G, Wang G D and Shu Y G 2018 *Chin. Phys. B* **27** 128701
[11] Liu C H, Liu T Y, Huang R Z, Gao T F and Shu Y G 2019 *Acta Phys. Sin.* **68** 240501 (in Chinese)
[12] Boyer P D 1997 *Annu. Rev. Biochem.* **66** 717
[13] Weber J and Senior A E 2003 *FEBS Lett.* **545** 61
[14] Abrahams J P, Leslie A G W, Lutter R and Walker J E 1994 *Nature* **370** 621
[15] Diez M, Zimmermann B, Börsch M, König M, Schweinberger E, Steigmiller S, Reuter R, Felekyan S, Kudryavtsev V, Seidel C A M and Gräber P 2004 *Nat. Struct. Mol. Biol.* **11** 135
[16] Nishi T and Forgac M 2002 *Nat. Rev. Mol. Cell. Biol.* **3** 94
[17] Yamato I, Kakinuma Y and Murata T 2016 *Biophys. Physicobiol.* **13** 37
[18] Yasuda R, Noji H, Kinosita K Jr and Yoshida M 1998 *Cell* **93** 1117
[19] Ueno H, Minagawa Y, Hara M, Rahman S, Yamato I, Muneyuki E, Murata T and Iino R 2014 *J. Biol. Chem.* **289** 31212
[20] Hayashi K, Watanabe H, Ueno H, Iino R and Noji H 2010 *Phys. Rev. Lett.* **104** 218103
[21] McMillan D G G, Watanabe R, Ueno H, Cook G M and Noji H 2016 *J. Biol. Chem.* **291** 23965
[22] Noji H, Yasuda R, Yoshida M, Kinosita K and Itoh H 2001 *J. Biol. Chem.* **276** 25480
[23] Uenno H, Suzuki K and Murata T 2018 *Cell Mol. Life Sci.* **75** 1789
[24] Noji H, Yasuda R, Yoshida M and Kinosita K Jr 1997 *Nature* **386** 299
[25] Iida T, Minagawa Y, Ueno H, Kawai F, Murata T and Iino R 2019 *J. Biol. Chem.* **294** 17017
[26] Watanabe R and Noji H 2014 *Nat. Commun.* **5** 3486
[27] Nelson M T, Humphrey W and Schulten K 1996 *Comput. Appl.* **10** 251
[28] Lindorff-Larsen K, Piana S, Palmo K, Maragakis P, Klepeis J L, Dror R O and Shaw D E 2010 *Proteins: Struct. Funct. Bioinf.* **78** 1950
[29] Arai S, Saijo S, Suzuki K, Mizutani K, Kakinuma Y, Ishizuka-Katsura Y and Murata T 2013 *Nature* **493** 703
[30] Darden T, York D and Pedersen L 1993 *J. Chem. Phys.* **98** 10089
[31] Bussi G, Donadio D and Parrinello M 2007 *J. Chem. Phys.* **126** 014101
[32] Parrinello M and Rahman A 1981 *J. Appl. Phys.* **52** 7182
[33] Dai L and Yu J 2020 *Biochem. Biophys. Res. Commun.* **533** 97
[34] Schlitter J, Engels M and Kruger P 1994 *J. Mol. Graph.* **12** 84
[35] Cheng X, Wang H and McCammon J A 2006 *PLOS Comput. Biol.* **2** e134
[36] Ovchinnikov V and Karplus M 2012 *J. Phys. Chem. B* **116** 8584
[37] Kenzaki H, Koga N, Hori N, Kanada R, Li W, Okazaki K I, Yao X Q and Takada S 2011 *J. Chem. Theory. Comput.* **7** 1979
[38] Clementi C, Nymeyer H and Onuchic J N 2000 *J. Mol. Biol.* **298** 937
[39] Okazaki K I, Koga N, Takada S, Onuchic J N and Wolynes P G 2006 *Proc. Natl. Acad. Sci. USA* **103** 11844
[40] Chao E, Dai L, Tian J, Da L T and Yu J 2022 *J. Vis. Exp.* **181** e63406
[41] Pearson K 1896 *Philos. Trans. R. Soc. A* **187** 253
[42] Dai L, Flechsig H and Yu J 2017 *Biophys. J.* **113** 1440
[43] Higgins D G, Bleasby A J and Fuchs R 1992 *Comp. Appl. Biosci.* **8** 189
[44] Gouet P, Courcelle E, Stuart D I and Métoz F 1999 *Bioinformatics* **15** 305